Early Paleogene evolution of terrestrial climate in the SW Pacific, Southern New Zealand

Richard D. Pancost, Kyle W. R. Taylor, and Gordon N. Inglis
Organic Geochemistry Unit, Bristol Biogeochemistry Research Centre and Cabot Institute, School of Chemistry, University of Bristol, Cantock's Close, Bristol BS8 1TS, UK (r.d.pancost@bristol.ac.uk)

Elizabeth M. Kennedy
Department of Paleontology, GNS Science, Lower Hutt, New Zealand

Luke Handley
Organic Geochemistry Unit, Bristol Biogeochemistry Research Centre and Cabot Institute, School of Chemistry, University of Bristol, Bristol, UK

Christopher J. Hollis and Erica M. Crouch
Department of Paleontology, GNS Science, Lower Hutt, New Zealand

Jörg Pross
Paleoenvironmental Dynamics Group, Institute of Geosciences, Goethe University Frankfurt, Frankfurt, Germany

Biodiversity and Climate Research Centre, Frankfurt, Germany

Now at Institute of Geosciences, Heidelberg University, Heidelberg, Germany

Matthew Huber
Earth and Atmospheric Sciences, Purdue University, West Lafayette, Indiana, USA

Stefan Schouten
Royal Netherlands Institute for Sea Research, Department of Marine Organic Biogeochemistry, Den Burg, Netherlands

Paul N. Pearson
School of Earth and Ocean Sciences, Cardiff University, Cardiff, UK

Hugh E. G. Morgans and J. Ian Raine
Department of Paleontology, GNS Science, Lower Hutt, New Zealand

[1] We present a long-term record of terrestrial climate change for the Early Paleogene of the Southern Hemisphere that complements previously reported marine temperature records. Using the MBT'-CBT proxy, based on the distribution of soil bacterial glycerol dialkyl glycerol tetraether lipids, we reconstructed mean annual air temperature (MAT) from the Middle Paleocene to Middle Eocene (62–42 Ma) for southern New Zealand. This record is consistent with temperature estimates derived from leaf fossils and palynology, as well as previously published MBT'-CBT records, which provides confidence in absolute temperature estimates. Our record indicates that through this interval, temperatures were typically 5°C warmer than those of today at such latitudes, with more pronounced warming during the Early Eocene Climate Optimum (EECO; ~50 Ma) when MAT was ~20°C. Moreover, the EECO MATs

are similar to those determined for Antarctica, with a weak high-latitude terrestrial temperature gradient (∼5°C) developing by the Middle Eocene. We also document a short-lived cooling episode in the early Late Paleocene when MAT was comparable to present. This record corroborates the trends documented by sea surface temperature (SST) proxies, although absolute SSTs are up to 6°C warmer than MATs. Although the high-calibration error of the MBT′-CBT proxy dictates caution, the good match between our MAT results and modeled temperatures supports the suggestion that SST records suffer from a warm (summer?) bias, particularly during times of peak warming.

1. Introduction

[2] Multiple proxy approaches to Paleogene marine temperature reconstruction reveal a relatively stable Paleocene followed by long-term warming through the Early Eocene, punctuated by several brief hyperthermals, the most widely studied being the Paleocene Eocene Thermal Maximum (PETM, ∼55.5 Ma) [*Zachos et al.*, 2001, 2008; *Sluijs et al.*, 2010]. Peak warmth in the Early Eocene Climate Optimum (EECO), ∼53 to ∼49 Ma [*Lear et al.*, 2000; *Zachos et al.*, 2008; *Bijl et al.*, 2009; *Hollis et al.*, 2009, 2012], was likely associated with the highest pCO_2 levels of the last 66 Ma [*Pearson and Palmer*, 2000; *Beerling and Royer*, 2011; *Pagani et al.*, 2005]. Subsequently, global temperatures began the long decrease that culminated in the current icehouse climate mode [*Lear et al.*, 2000; *Zachos et al.*, 2008; *Bijl et al.*, 2009; *Hollis et al.*, 2012].

[3] Establishing the pattern of global climate change through the Paleogene depends on compiling robust surface temperature estimates from representative regions and latitudes. Recently, a suite of Paleogene sea surface temperature (SST) estimates have been generated for the SW Pacific [*Burgess et al.*, 2008; *Bijl et al.*, 2009; *Hollis et al.*, 2009, 2012; *Liu et al.*, 2009; *Creech et al.*, 2010; *Sluijs et al.*, 2012] using the TEX_{86} proxy (TetraEther indeX of glycerol dialkyl glycerol tetraethers, GDGTs, containing 86 carbon atoms

[*Schouten et al.*, 2002]), alkenones [*Liu et al.*, 2009], and oxygen isotopes and Mg/Ca ratios derived from planktic foraminifera. These have generated much interest, because in tandem with tropical records they can be used to evaluate how latitudinal temperature gradients have changed over geological time [e.g., *Bijl et al.*, 2009].

[4] However, the high absolute temperatures from these records have been questioned [*Pagani et al.*, 2011; *Hollis et al.*, 2012]. One issue of concern has been a large and unexpected offset, especially in the SW Pacific, between two different GDGT-based SST proxies: TEX_{86}^H and TEX_{86}^L; these proxies are expected to yield similar values in these settings [*Kim et al.*, 2010]. TEX_{86}^H-derived SSTs are also higher than those derived from oxygen isotopes in well preserved, co-occurring planktonic foraminifera [*Burgess et al.*, 2008; *Hollis et al.*, 2012]. Although these records do track the deep water temperature trends recorded by benthic foraminifera [*Cramer et al.*, 2011; *Zachos et al.*, 2008], the TEX_{86}^H-derived SSTs are inconsistent with climate models and some proximal terrestrial temperature estimates [*Hollis et al.*, 2009; *Huber and Caballero*, 2011]. *Hollis et al.* [2012] discussed these issues and concluded that the proxy data could be reconciled with modeled SSTs through conservative application of calibration equations, including use of the TEX_{86}^L calibration, adjustment for a likely summer bias, and consideration of the likely influence of southward

expansion of tropical surface waters during times of peak warming. A crucial test for these conclusions is to examine how they conform with alternative approaches to high-latitude temperature reconstructions, and especially parallel terrestrial temperature records.

[5] We use the distribution of branched GDGTs, derived from soil bacteria, to estimate mean annual air temperature (MAT) using sediments from two marine sections within the Canterbury Basin, eastern New Zealand (Mid-Waipara River and Hampden Beach), previously described by *Hollis et al.* [2012]. The record represents a long-term terrestrial temperature record, the first that extends from the Middle Paleocene to Middle Eocene, and it complements other, recently published branched GDGT-derived MAT records from the SW Pacific and Antarctic margin [*Pross et al.*, 2012; *Bijl et al.*, 2013] as well as previous marine temperature reconstructions for these sections [*Burgess et al.*, 2008; *Hollis et al.*, 2009, 2012; *Creech et al.*, 2010]. The degree of branching in non-isoprenoidal GDGTs in soils, expressed as the MBT′ ratio (methylation index of branched tetraethers), is related to pH and MAT [*Peterse et al.*, 2012; *Weijers et al.*, 2007a]. The CBT ratio (cyclization index of branched tetraethers) is related to pH and can be used to remove the pH impact on the MBT record [*Peterse et al.*, 2012; *Weijers et al.*, 2007a]. When determined for marine sediments, the MBT′-CBT proxy [*Peterse et al.*, 2012] is inferred to record MAT of the source catchment, in this case, southern New Zealand. We compare our MBT′-CBT estimates for MAT with those derived from analyses of leaf fossil assemblages, including a new record from Otaio Gorge (Canterbury Basin), and terrestrial palynomorphs, as well as the MAT and SST records noted above.

2. Methods

2.1. Site Description

2.1.1. Mid-Waipara River
[6] Sedimentary rock samples were collected at two sections (Figure 1) from the Mid-Waipara River section, located in the northern Canterbury Basin (Figure 2): a Lower to Upper Paleocene section through the Loburn Formation and Waipara Greensand, capped by basal Eocene Ashley Mudstone (Column 2) [*Hollis et al.*, 2012] and a Lower to Middle Eocene section of Ashley Mudstone (Column 4) [*Morgans et al.*, 2004]. The basal Eocene in Column 2 was correlated with the

PETM by *Hollis et al.* [2012]. The Mid-Waipara River Paleocene to Eocene sequence was deposited at upper bathyal depths during long-term transgression linked to basinal subsidence at a passive margin [*King et al.*, 1999]. Neritic conditions and proximity to land are indicated by the scarcity of planktic foraminifera and a high proportion of terrestrial palynomorphs.

2.1.2. Hampden Beach
[7] The Hampden Beach section is located in the southern part of the Canterbury Basin (Figure 1). We use the same sample suite reported by *Hollis et al.* [2012] with the stratigraphy described by *Morgans* [2009]. The sample suite comprises two samples from the Lower to Middle Eocene Kurinui Formation and 10 samples from an interval spanning four climate cycles in the Middle Eocene Hampden Formation [*Burgess et al.*, 2008].

2.1.3. Otaio River
[8] We complement our MBT′-CBT proxy data with climate reconstruction based on a leaf fossil assemblage from the Otaio River Gorge section (Figure 1). Paleogene strata crop out along the Otaio River Gorge, southwest of Timaru [*Forsyth*, 2001]. Plant macrofossils have been recovered from a mudstone unit within coal measures of the Paleocene-Eocene Broken River Formation. A palynology sample from the matrix of the leaf-rich unit indicates a correlation with pollen zone PM3b (= earliest Eocene). The presence of dinoflagellate cysts and evidence of burrowing in the surrounding mudstone suggests estuarine deposition of the leaves. The genus *Apectodinium* dominates the dinocyst assemblages in this unit, providing additional support for an earliest Eocene age [*Crouch and Brinkhuis*, 2005]. Preliminary carbon isotope data supports correlation with the PETM. Leaf-morphology-based paleoclimate analyses have been applied to the leaf assemblage in this unit; GDGTs were not present due to the elevated thermal maturity of these sediments.

2.1.4. Age Control
[9] Age control for all sections is based on biostratigraphy, which has been recalibrated to the 2012 geological time scale [*Gradstein et al.*, 2012; *Crouch et al.*, 2013].

2.2. Organic Geochemistry

[10] Samples were gently washed with methanol and powdered with a Retsch PM100 Ball Mill. Total organic carbon, inorganic carbon, sulfur, and total nitrogen were measured as a mass % of the total sediment using a Carlo Erba EA 1108 and a
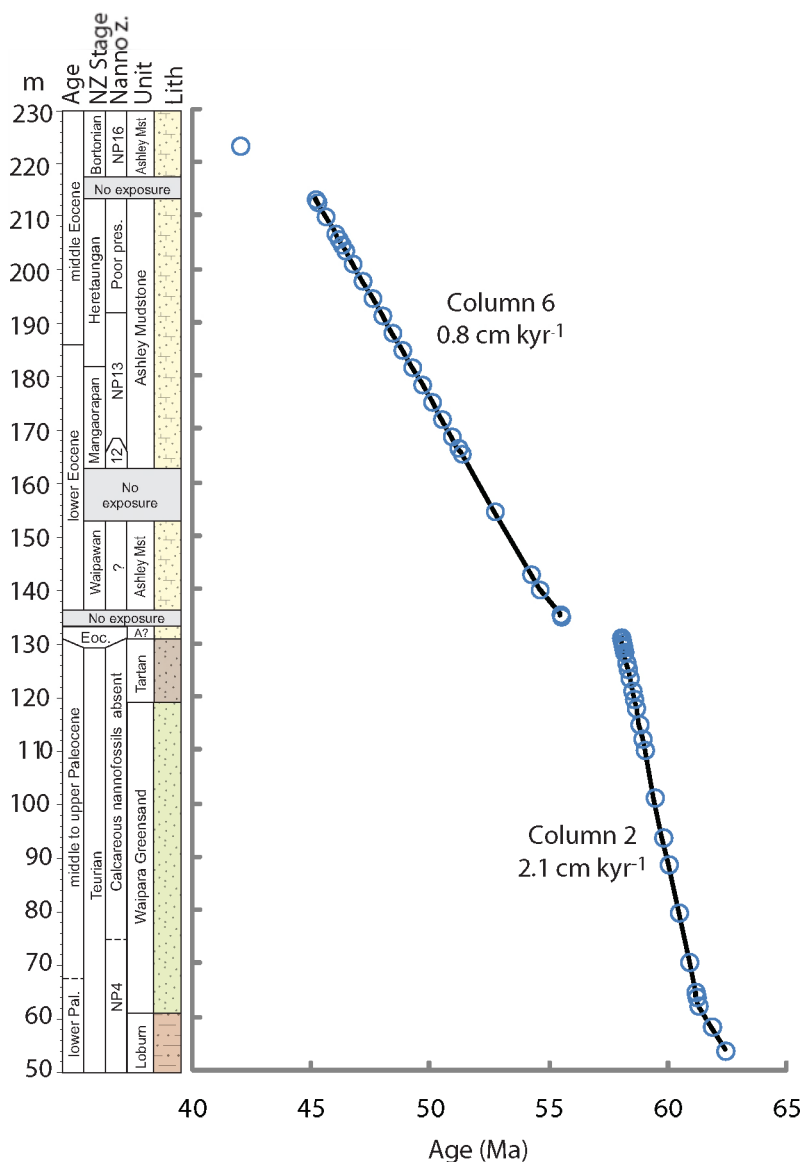
Figure 1. Generalized lithological log, NZ, and international time scale [*Gradstein et al.*, 2012] for columns 2 and 6 from the Mid-Waipara River Section. Blue circles represent samples. Note the three intervals of nonexposure.

Coulomat 702 (Strohlein). Powdered samples were extracted via Soxhlet apparatus for 24 h using dichloromethane/methanol (2:1 v/v) as the organic solvent. The total lipid extracts were separated into two fractions on an aminopropyl solid phase extraction column by elution with dichloromethane/iso-propanol (3:1 v/v; neutral fraction) and 2% (by volume) acetic acid in diethyl ether (acid fraction). The neutral fraction was further split using a column packed with (activated) alumina by elution with hexane (saturated hydrocarbon fraction), hexane/dichloromethane (9:1 v/v; aromatic fraction) and dichloromethane/methanol (1:2 v/v; polar fraction).

[11] Individual compounds were identified and quantified relative to internal standards using gas chromatography (GC) and gas chromatography-mass spectrometry (GC-MS). Prior to analyses, acid fractions were methylated using BF_3/MeOH and polar and acid fractions were silylated with BSTFA (*N,O*-bis(trimethylsilyl)trifluoroacetamide). GC analysis was performed on a CarloErba Gas Chromatograph equipped with a flame ionization detector (FID) and fitted with a Chrompack fused silica capillary column (50 m $\times$ 0.32 mm i.d.) coated with CP Sil-5CB stationary phase (dimethyl-polysiloxane equivalent, 0.12 μm film thickness); GC-MS analysis was performed on a Thermoquest
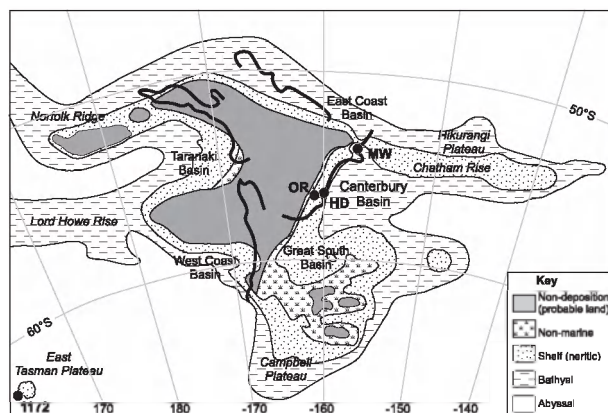
Figure 2. Palinspastic reconstruction for New Zealand region in the Early Eocene [from *Hollis et al.*, 2012], showing reconstructed location of the mid-Waipara River (MW), Hampden Beach (HD), and Otaio River (OR) sections. Also shown is IODP Site 1172, from which similar TEX_{86}-SSTs (and Eocene MATs) have been obtained [*Bijl et al.*, 2013].

Finnigan Trace GC interfaced with a Thermoquest Finnigan Trace MS operating with an electron ionization source at 70 Ev and fitted with a fused silica capillary column (50 m × 0.32 mm i.d.) coated with ZB1 stationary phase (dimethylpolysiloxane equivalent, 0.12 μm film thickness), scanning over m/z ranges of 50–850 Da. For both GC and GC-MS, 1 μL of sample was injected at 50°C using an on-column injector. Temperature was increased to 130°C with an initial ramp of 20°C/min, then to 300°C at 4°C/min, followed by an isothermal for 20 min.

[12] The polar fractions, containing the GDGTs, were dissolved in hexane/iso-propanol (99:1, v/v) and passed through 0.45 μm PTFE filters. Fractions were analyzed by high-performance liquid chromatography/atmospheric pressure chemical ionization-mass spectrometry (HPLC/APCI-MS) using an Agilent 1100 series/Hewlett Packard 1100 MSD. Normal phase separation was achieved on an Alltech Prevail Cyano column (150 mm × 2.1 mm; 3 μm i.d.) with a flow rate of 0.2 mL min^{-1}. Initial solvent was hexane/iso-propanol 99:1 (v/v), eluted isocratically for 5 min, followed by a linear gradient to 1.8% iso-propanol over 45 min. Analyses were performed in selective ion monitoring mode (SIM) to increase sensitivity and reproducibility and $[M+H]^+$ (protonated molecular ion) GDGT peaks were integrated. The ratio of branched GDGTs to crenarchaeol in marine and lacustrine sediments is a function of soil organic matter input, expressed as the Branched versus Isoprenoid Tetraether (BIT) index [*Hopmans et al.*, 2004]:

$$BIT = ([VI]+[VII]+[VIII])/([VI]+[VII]+[VIII]+[IV]) \quad (1)$$

[13] Numerals refer to individual GDGT structures shown in Figure 3. TEX_{86}-derived sea surface temperatures (SST) were reported previously [*Hollis et al.*, 2012] and are based on both the high (GDGT index 2; log of TEX_{86}^H) and low (GDGT index 1; log of TEX_{86}^L) temperature equations of *Kim et al.* [2010]. The degree of cyclization and branching in non-isoprenoidal terrestrial GDGTs, expressed as CBT (cyclization index of branched tetraethers) and MBT (methylation index of branched tetraethers), are related to pH and mean air temperature (MAT) according to the empirically derived relationships first defined by *Weijers et al.* [2007b] based on a global soil data set and then refined by *Peterse et al.* [2012] for an expanded data set; we use the latter here:

$$CBT = -\log\ [([VIb]+[VIIb]/[VI]+[VII])] \quad (2)$$

$$pH = 7.9 - 1.97\ CBT\ (r^2 = 0.70) \quad (3)$$

$$MBT' = ([VI]+[VIb]+[VIc])/([VI]+[VIb]+[VIc]+[VII] \\ +[VIIb]+[VIIc]+[VIII]) \quad (4)$$

[14] Note that [VIIIb] and [VIIIc] are included in the denominator of the original MBT term [*Weijers et al.*, 2007] but are omitted from the revised calibration. The new approach yields MAT according to:

$$MAT(°C) = 0.81 - 5.61 \times CBT + 31 \times MBT' \quad (5)$$

[15] Equation (5) is typically defined as the MBT'-CBT proxy, and the root mean square error in the revised calibration is ±4.9°C. We have also recalculated the MATs previously published for the Wilkes Land basin, East Antarctic Margin (Integrated Ocean Drilling Program, ODP Expedition 318, Site U1356) [*Pross et al.*, 2012] using the *Peterse et al.* [2012] calibration.

2.3. Temperature and Precipitation Estimates Derived From Sporomorph Assemblages

[16] Temperature and precipitation estimates were also obtained from selected Paleocene and Early Eocene sporomorph assemblages in the Mid-Waipara River section (Column 2 and Column 6, respectively), and from an earliest Eocene assemblage from the matrix of the Otaio River leaf flora. Samples were coarsely crushed and processed using
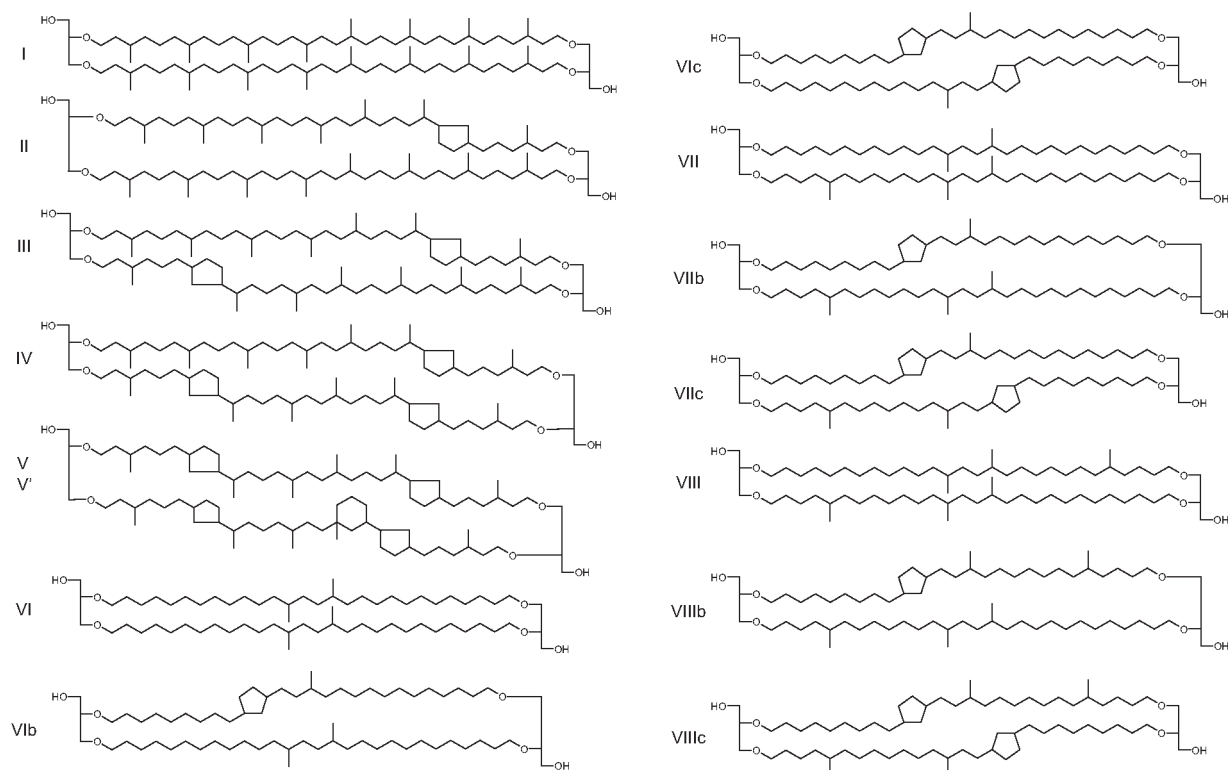
Figure 3. Isoprenoidal (I–V) and non-isoprenoidal (VI–VIII) GDGTs used to reconstruct SST, MAT, pH, and BIT indices.

conventional palynological techniques, including treatment with hydrochloric acid to remove carbonates, hydrofluoric and hydrochloric acids to remove silicates, oxidation using 36% nitric acid, removal of humic material with 5% ammonia solution, flotation using 2.0 s.g. heavy liquid, and sieving on 6 μm filter cloth before glycerine jelly strew mounting of residues for microscopic examination. For each sample approximately 200 sporomorphs were initially counted, and then the remainder of two slides was scanned for less common species.

[17] Bioclimatic analyses using the nearest living relative method [*Greenwood et al.*, 2005] were used to reconstruct MAT and mean annual precipitation (MAP). The results were compared with those derived from the coexistence approach of *Mosbrugger and Utescher* [1997]. For both approaches, fossil sporomorph taxa are identified and characterized based on their nearest living relatives [*Pross et al.*, 2012; *Contreras et al.*, 2013]. Climate parameters are derived from the assemblage of nearest living relatives. The climatic requirements of the nearest living relatives are determined using the same sources and are therefore identical for the two approaches; specifically, they are derived from (i) the data set of *Pross*

et al. [2012], which is mainly based on distribution data from the Australian National Herbarium online database [*Australian National Herbarium Specimen Information Register*, 2011] and the mathematical climate surface software ANUCLIM 5.156 [*Houlder et al.*, 1999], and (ii) the Palaeoflora database, which contains climatic information for plant taxa based on their global distribution [*Utescher and Mosbrugger*, 2013]. Also, the climate estimates through the bioclimatic analyses and the coexistence approach are based on the evaluation of the same taxa (compare supporting information Table S2[1]).

[18] An 80% confidence interval defines the climate envelope derived from bioclimatic analysis. The coexistence approach sensu *Mosbrugger and Utescher* [1997] aims to derive a coexistence interval for a specific climate parameter in which a maximum number of nearest living relatives of a given flora coexist. The limits of this coexistence interval are defined by the minimum and maximum values. Taxa whose climate profiles are not within the zone of overlap of the majority of taxa are considered

---

[1]Additional supporting information may be found in the online version of this article.

outliers and have been excluded. The width of a coexistence interval determines the resolution of the coexistence approach for a given climate parameter. This interval width tends to increase in proportion to the number of nearest living relatives identified [*Mosbrugger and Utescher*, 1997; *Pross et al.*, 2000]. The two methods yield consistent results for the climate parameters evaluated, indicating that our reconstructions are robust.

2.4. Temperature Estimates From the Otaio River Leaf Flora

[19] Two forms of leaf-morphology-based paleoclimate analysis were applied to the Otaio leaf flora: Leaf Margin Analysis (LMA) [e.g., *Wing and Greenwood*, 1993] and Climate Leaf Analysis Multivariate Program (CLAMP) [e.g., *Wolfe*, 1993; *Spicer et al.*, 2009]. Both of these methods only include leaves from woody dicotyledonous angiosperms (dicots) in these analyses. LMA is a univariate method involving assessment of margin character for each leaf morphotype, and application of regression equations relating margin type (% species or leaf morphotypes within an assemblage with entire margins) to MAT based on modern analogue data. The Otaio Gorge assemblage consists of 18 morphotypes with an entire-margined percentage of 66.7%. Various LMA calibrations now exist for calculating mean annual temperature (MAT), and two of these LMA calibrations were applied here. The first is based on a southeast Asian modern data set collected by *Wolfe* [1979]; the regression equation was later published by *Wing and Greenwood* [1993]. The second LMA regression equation is based on Australian modern data collated by *Greenwood et al.* [2004], with a data set comprising 74 sites, each of which has greater than 20 species of woody dicots.

[20] CLAMP is a further development of LMA and involves measuring the leaf morphotypes for 31 leaf character variables and produces estimates for multiple climate parameters. The CLAMP method is based on large modern analogue data sets of leaf character information and associated climate information collected using CLAMP-defined protocols. CLAMP analysis was performed by adding the Otaio percentage scores to the standard Physg3brcAZ calibration data set and analyzing with the associated Met3brAZ climate data set using the CCA function of CANOCO [*ter Braak*, 1986]. Climate estimates were determined by projecting the positioned Otaio flora onto each of 11 climate vectors using the standard CLAMP

results spreadsheet from the CLAMP website (http://clamp.ibcas.ac.cn/Clampset2.html).

3. Results and Discussion

3.1. Biomarkers Present in Mid-Waipara River and Hampden Beach Sediments

[21] As documented previously [*Burgess et al.*, 2008; *Hollis et al.*, 2009, 2012], the Mid-Waipara River and Hampden Beach sections are characterized by relatively thermally immature organic matter derived from a mixture of marine and terrestrial sources. The saturated hydrocarbon and acid fractions of all Mid-Waipara and Hampden Beach sediments contain a homologous series of *n*-alkanes and *n*-alkanoic acids (Figure 4), likely derived from the leaf waxes of terrestrial higher plants [*Eglinton et al.*, 1962; *Kolattukudy*, 1976; *Reiley et al.*, 1991]. Confirmation of a higher plant origin of *n*-alkanes is provided by the odd-over-even carbon number predominance (OEP) of *n*-alkanes in a homologous series [*Scalan and Smith*, 1970]: $OEP = (C_{n-2} + 6 \times C_n + C_{n+2})/(4 \times C_{n-1} + 4 \times C_{+1})$, with $n = 27$. In the acid fraction, the high molecular weight (HMW) *n*-alkanoic acids are dominated by even carbon number homologues, particularly the C_{30} and C_{32} components in Paleocene sediments and the C_{28} and C_{30} components in Eocene sediments, all indicative of a typical higher plant signature [*Reiley et al.*, 1991]. The alcohol fraction contains *n*-alkanols, also likely derived from higher plant leaf waxes; also present are C_{27-29} sterols, as well as low concentrations of dinosterol derivatives, both consistent with marine algal inputs. The compounds of greatest interest for this study, however, are the glycerol dialkyl glycerol tetraether lipids which are the basis of various SST and MAT proxies. Hampden Beach sediments contain a similar distribution of biomarkers, including a strong contribution of *n*-alkyl components of likely leaf wax origin.

3.1.1. GDGT Distributions: MBT and CBT Ratios and MAT Trends

[22] Our reconstructed MATs are based on the MBT′ and CBT indices shown in Figure 5. MBT′ indices exhibit dramatic long-term variability through the section, with values generally being low in the Paleocene (0.5–0.6) and markedly higher (0.7–0.9) in the Eocene. CBT indices exhibit a similar overall range, but exhibit much greater sample-to-sample variability. Overall, CBTs increase from values of 0.5 in the Paleocene to 0.8 in the PETM interval at Mid-Waipara. They are then variable
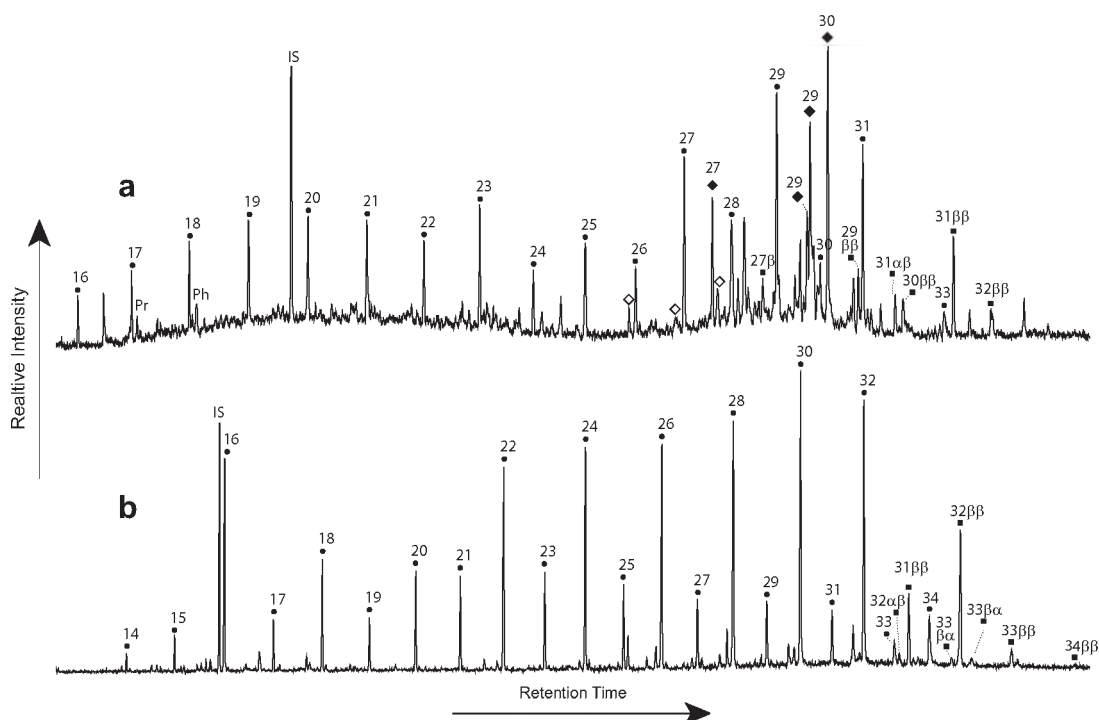
Figure 4. Partial gas chromatograms of typical Mid-Waipara Column 6 apolar (a) and acid (b) fractions. Solid circles denote *n*-alkanes and *n*-alkanoic acids in Figures 4a and 4b, respectively, with associated numerals indicating the number of carbon atoms. Numerals associated with black squares followed by Greek letters denote carbon number and C-17 and C-21 stereochemical configuration of hopanes and hopanoic acids in Figures 4a and 4b, respectively. Open and closed diamonds indicate sterenes and hopenes, respectively. In the apolar fraction, pr and ph indicate pristane and phytane.

through the overlying Eocene but generally increase to values of 0.9 and have values ranging from 0.85 to 0.93 in the high-resolution Middle Eocene Hampden Beach record.

[23] Collectively, the two indices can be used to calculate MAT. For comparison, temperatures obtained using both the original [*Weijers et al.*, 2007b] and the more recent [*Peterse et al.*, 2012] calibrations are shown in Figure 5. Both exhibit similar trends, although the latter yields lower MATs as has been observed elsewhere [*Peterse et al.*, 2012]. In general, the MAT trend parallels that of the MBT′ ratio, consistent with it being the primary driver in the MBT′-CBT calibration. The CBT component appears to exert little influence on the shape of the MAT reconstruction; however, because it does vary through the sequence, we tested its impact on our MAT estimates (Figure 5c) by calculating MAT using either minimum or maximum CBT values (0.5 and 0.9). These affected our calculated MATs by less than ±2°C.

[24] Overall, MAT ranges from 10 to 22°C ± 4.9°C through the section (Figure 5c), characterized by particularly warm temperatures, >20°C, during the PETM and late Early to early Middle Eocene. Coldest temperatures are recorded in the Paleocene (~15°C) and especially from 58 to 59 Ma where MAT falls to 10°C. Significantly, and in striking contrast to previously published SST records [*Bijl et al.*, 2009, 2013; *Hollis et al.*, 2009, 2012], the EECO does not stand out as being any warmer than the succeeding early Middle Eocene. Cooling only becomes evident in the late Middle Eocene.

3.1.2. Fidelity of MBT′-CBT-Derived MATs
[25] A variety of factors could affect the derived MBT′-CBT-derived MATs. An important factor is the location of the source area for the biomarkers. Given the study sites' proximal location to New Zealand and the lack of any other nearby land masses, our terrestrial signatures almost certainly derive from New Zealand. This is particularly true for the GDGTs; although they can be transported via dust [*Fietz et al.*, 2013], the concentrations are low and aeolian processes are not likely to be important in proximal settings [*Hopmans et al.*, 2004]. The vegetation composition derived from palynology is consistent with this interpretation, as there is no doubt that the palynomorphs are derived
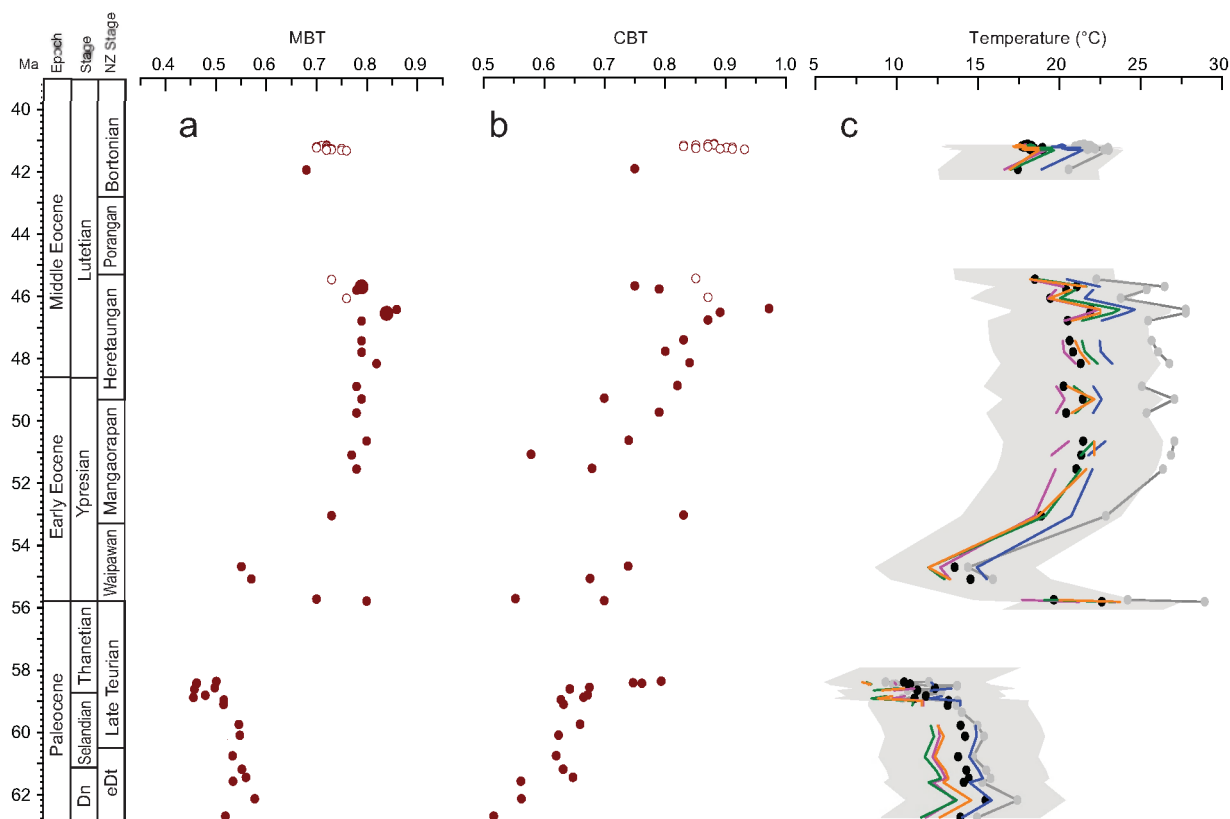
Figure 5. (a) MBT′ and (b) CBT indices, shown as closed circles (Waipara) and open circles (Hampden Beach). (c) MATs derived from various MBT-CBT calibrations, including the MBT′-CBT calibration of *Peterse et al.* [2012] in solid circles (with gray shaded region showing the ±4.9°C error) and original MBT-CBT calibration of *Weijers et al.* [2007b] in gray circles. Also shown are MATs derived from the Kilimanjaro regional calibration [*Sinninghe Damsté et al.*, 2008] (orange line), the Amazon regional calibration [*Bendle et al.*, 2010] (green line), and the *Peterse et al.* [2012] calibration but assuming constant high (magenta line) or low CBT values (blue line). Time scales show the international Paleocene and Eocene epochs and the corresponding New Zealand stages.

from the New Zealand landmass. However, a cool bias from an altitudinal effect cannot be ruled out [e.g., *Bendle et al.*, 2010]: palinspastic reconstruction suggests that Mid-Waipara deposition occurred at bathyal depths but also near to shore, and it is reasonable to assume that a moderately steep submarine depth gradient continued onshore.

[26] A further issue in the estimation of MAT from br-GDGTs is that regional calibrations [*Bendle et al.*, 2010; *Sinninghe Damsté et al.*, 2008] can differ significantly from the global calibration of *Weijers et al.* [2007b]. MATs derived from the two previously published regional soil calibrations, based on an altitudinal profile of Mt. Kilimanjaro, Kenya [*Sinninghe Damsté et al.*, 2008] and the Amazon catchment (*Bendle et al.* [2010], including the Amazon basin and Andean uplands), are shown in Figure 5c. Both yield MATs similar to those derived from the *Peterse et al.* [2012] calibration

(and lower temperatures than those derived from the *Weijers et al.* [2007], calibration), consistent with the conclusion of *Peterse et al.* [2012] that there is little regionality in their expanded data set. It is likely that some of the previously reported differences between regional and global calibrations document a limitation of the original data set [*Weijers et al.*, 2007b]. The limitations of the MBT′-CBT thermometer in arid regions [e.g., *Peterse et al.*, 2012; Yang et al., submitted] are unlikely to be relevant here (Table 1).

[27] Another concern with interpreting MAT from the Mid-Waipara section is the low BIT indices, which range from 0.06 to 0.3 (mean of 0.12). These indicate that our MAT estimates derive from a low abundance of branched GDGTs relative to marine (crenarchaeol) inputs and raises the possibility that the terrigenous br-GDGT distribution might be partially overprinted by in situ

Table 1. Temperatures and Precipitation Reconstructed From Bioclimatic and Coexistence Analysis of Sporomorphs

	46.1 Ma	46.7 Ma	51.3 Ma	51.6 Ma	55.5 Ma (Otaio Gorge)	58.5 Ma	58.6 Ma	58.7 Ma
Mean annual Temperature	18.2[a] (5.7)	22.6 (1.4)	17.4 (6.6)	22.6 (1.4)	17.4 (6.6)	17.4 (6.6)	17.4 (6.6)	10.9 (0.1)
	16.8[b] (6.2)	17.2 (6.6)	15.8 (7.5)	17.1 (6.8)	16.0 (6.0)	13.7 (3.4)	13.2 (2.7)	12.0 (1.7)
Mean annual Precipitation	1420[a] (200)	1070 (140)	1420 (198)	1420 (200)	1090 (160)	1550 (310)	1080 (150)	1550 (310)
	1270[b] (530)	1250 (500)	1180 (640)	1260 (560)	1140 (480)	1410 (710)	1330 (610)	1440 (740)

[a]Mid value from coexistence approach (with range in parentheses).
[b]Estimate from bioclimatic analysis (with error in parentheses).

sedimentary production [*Peterse et al.*, 2009; *Zhu et al.*, 2011]. To explore this further, we compare the SST (TEX_{86}^L)-MAT difference to BIT indices (Figure 6), assuming that (a) in situ production at the seafloor would yield anomalously low MATs and (b) that would be recorded by deviations from independent temperature reconstructions. Only a weak relationship is observed for BIT values between 0.1 and 0.3 and SST-MAT differences are typically 0–3°C in that range. In contrast, for sediments with BIT values below 0.1, the temperature difference is larger. For four samples in the earliest Eocene, with BIT values lower than 0.08, the temperature difference >7°C (Figure 7a). As these samples do not have anomalously high pH values, this could be a true difference, perhaps reflecting higher-altitude sources for branched GDGTs in post-PETM New Zealand. This could also explain why the temperature difference is not evident in a

comparable SST-MAT comparison (Figure 7a) from ODP Site 1172 [*Bijl et al.*, 2013]. Regardless of the underlying causes of these differences, we do not discuss these Early Eocene data further.

[28] The in situ marine production of GDGTs likely had a relatively minor impact on the rest of the record. Despite low BIT indices, the sediments contain abundant terrestrial biomarkers (see above) and terrestrial palynomorphs (over 50% of the total palynomorph assemblage in the Paleocene and Middle Eocene and ~30% in the Early Eocene), and LC-MS analyses yield strong signals for br-GDGTs. Moreover, *Peterse et al.* [2009] and *Zhu et al.* [2011] noted that in situ marine production of br-GDGTs is associated with excess abundances of GDGT VIc and VIIc, which gives rise to elevated pH estimates. As none of these features are evident in our data set, in situ production is considered to have been negligible. Even so, the low BIT values, together with the high calibration error, indicate that minor temperature variations should not be considered significant.

3.2. Comparison of Temperature Records

[29] These MBT'-CBT data represent the first long-term terrestrial temperature record for the middle latitude Paleogene. In order to corroborate the record, we compare it to local MAT estimates derived from leaf fossil assemblages and palynology and previously published SST records. We then present a model for the Early Paleogene evolution of SW Pacific climate based on the sum of all records.

3.2.1. Comparison of MATs Derived From Geochemical, Palynological, and Paleobotanical Approaches

[30] Palynological data indicate a mesothermal-microthermal regime (temperate) for the early Late Paleocene, with palynofloras dominated by podocarps such as *Phyllocladites mawsoni* and *Podocarpidites* spp. Converting these assemblages to MAT using bioclimatic analysis yields a range of 12–13.5°C (10–17°C with one standard error; Table 1), which is consistent with MATs derived
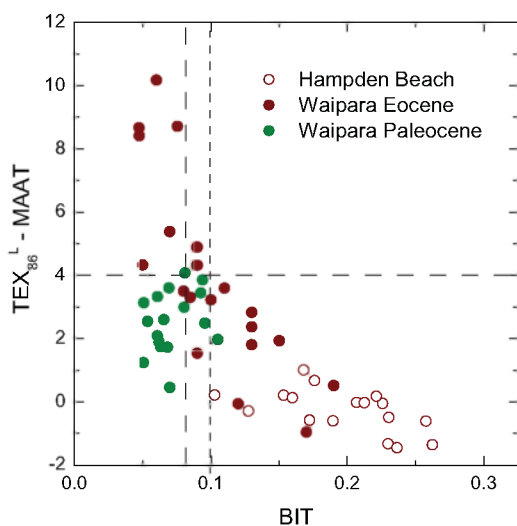

Figure 6. Crossplot of BIT indices against the difference between TEX_{86}^L-derived SSTs and MBT'-CBT-derived MATs. The horizontal dashed line at 4°C, above which we would interpret our data cautiously, is conservative as the combined calibration error for the respective proxies is larger. The vertical dashed lines denote apparent threshold BIT indices of 0.1 and 0.08, below which the range in ΔTemperature becomes much larger.
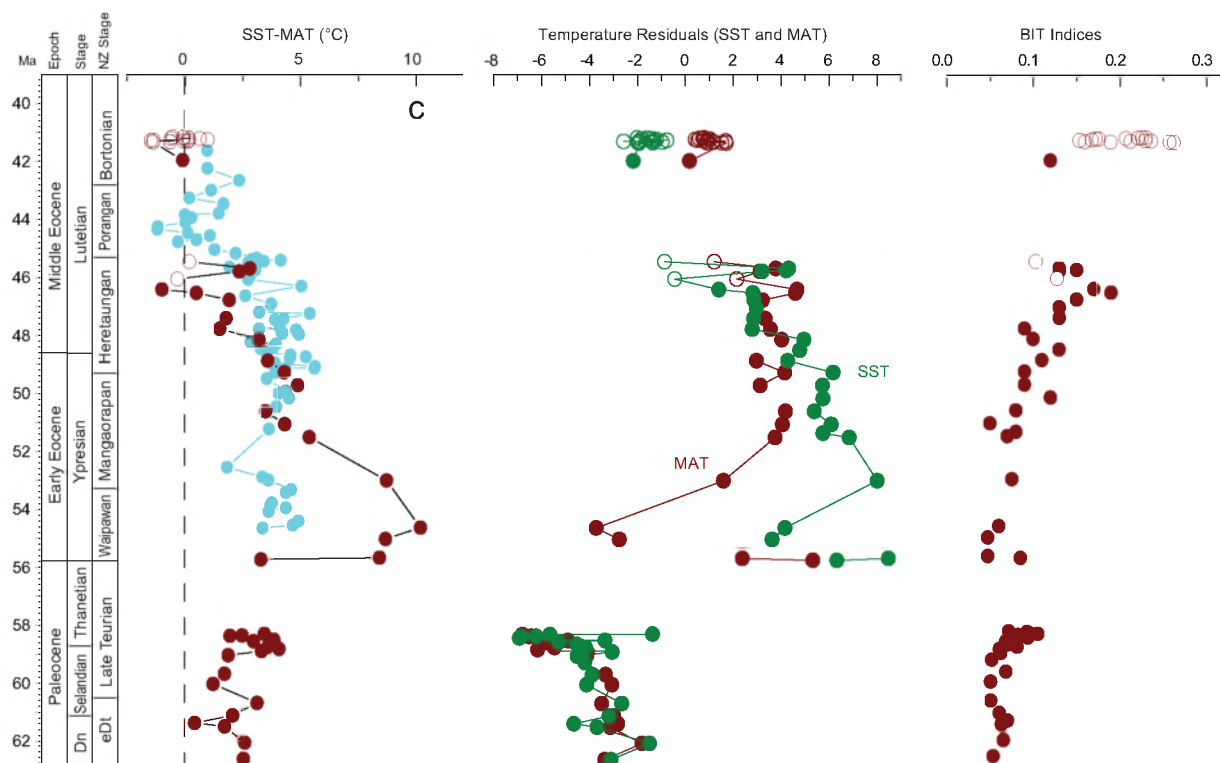
Figure 7. Relationships between TEX_{86}^L-derived SSTs and MBT'-CBT-derived MATs in the mid-Waipara (closed circles) and Hampden Beach sections (open circles). In (a), the differences between SST and MAT absolute values are shown; also shown by blue circles are the differences for ODP Site 1172 [*Bijl et al.*, 2013]. In (b), SST (green) and MAT (red) data are plotted as temperature residuals from the respective mean values of the entire record. For comparison, BIT indices are shown in (c).

from MBT'-CBT indices (Figure 8b). Temperature estimates based on physiognomic analysis of leaf fossils are restricted to probable Early Paleocene assemblages from western South Island [*Kennedy*, 2003], where three assemblages each comprising >20 leaf forms yield a slightly lower MAT range (including standard error) of 7.5–12.3°C based on CLAMP and 4.7–10.4°C based on LMA, both implying a microthermal regime (MAT <12°C).

[31] During the PETM, EECO, and early Middle Eocene, GDGT-derived MATs of 20–22°C indicate cool subtropical conditions. These are similar to MBT'-CBT temperatures obtained for Site 1172 [*Bijl et al.*, 2013] across the same interval and for the Wilkes Land basin during the EECO [*Pross et al.*, 2012] (Figure 8b). In New Zealand, floral analyses for the EECO indicate a mesothermal-megathermal regime, with palynoflora dominated by Casuarinaceae (*Myricipites harrisii*) and Proteaceae [*Pocknall*, 1990; *Raine et al.*, 2009; *Crouch and Brinkhuis*, 2005] and consistent with warm temperate to subtropical conditions. Subtropical conditions are also consistent with the occurrence

of mangrove pollen (*Nypa*) and the thermophilous taxa *Cupanieidites* and *Anacolosidites* [*Mildenhall*, 1980]. Bioclimatic analyses of these assemblages yield temperatures of 16–17°C (9–24°C including one standard error). Thus, these temperatures are lower than the MBT'-CBT-derived estimates but within the error range (Figure 8b).

[32] There are few published Eocene temperature estimates based on physiognomic analysis of New Zealand leaf fossils. A probable earliest Eocene dicot leaf assemblage from Kakahu, South Canterbury, produced cool temperate MAT estimates (LMA-based; Australian and SE Asian calibrations), but the very low diversity of the assemblage (12 morphotypes) means these estimates have high uncertainty [*Pole*, 1997, 2010]. The general physiognomy (leaf margin and leaf size) of a similarly low diversity (13 morphotypes) Early to Middle Eocene dicot leaf flora from Livingstone, North Otago, suggested a warmer climate [*Pole*, 1994]. We have analyzed the Otaio dicot leaf collection, tentatively placed within the PETM (see section 2.1.3). LMA (based on the SE Asian calibration)
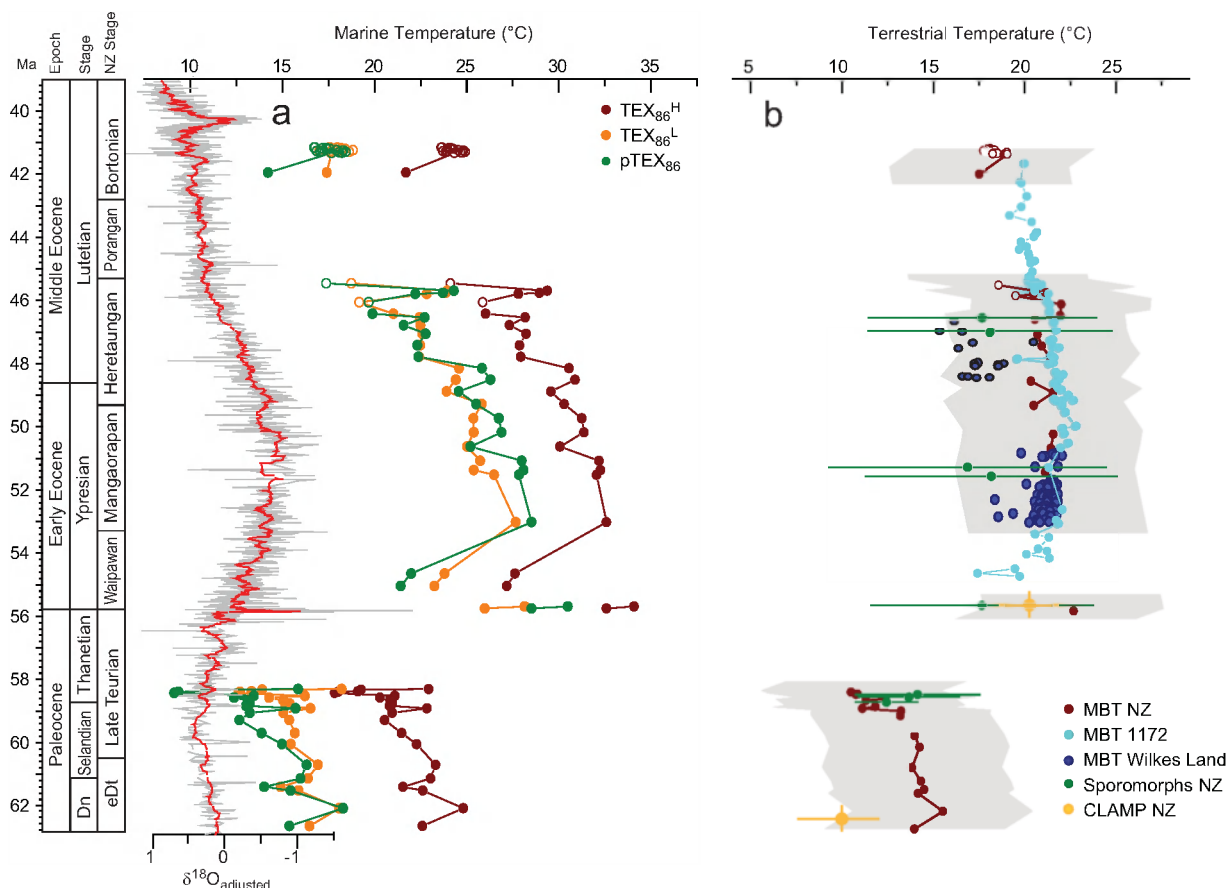
Figure 8. Temperature records from the Mid-Waipara River (closed circle) and Hampden Beach (open circle) sections. (a) The global benthic foraminiferal $\delta^{18}O$ stack (compiled by *Cramer et al.* [2011]; gray line, with red line being the 30-point moving average; note not scaled to temperature) and TEX_{86}^H- and TEX_{86}^L- derived SST records (from *Hollis* [2012], and based on the calibrations of *Kim et al.* [2010]) for New Zealand spanning the Early Paleocene to Middle Eocene; also shown (in green) are $pTEX_{86}$ reconstructions [*Hollis et al.*, 2012]. (b) Reconstructed mean annual air temperatures derived from MBT'-CBT indices and the global calibration of *Peterse et al.* [2012] from: Mid-Waipara River and Hampden Beach (red), IODP Site U1356 (Wilkes Land margin, dark blue) [*Pross et al.*, 2012], and ODP Site 1172 (light blue) [*Bijl et al.*, 2013]. The shaded gray region denotes the ±4.9°C error bars around the New Zealand data only. Green data are MATs based on bioclimatic analysis of sporomorph assemblages from the Mid-Waipara River section (except for PETM datum, which is from Otaio Gorge), and the orange data represent MAT estimates (20.0 ± 2.4°C) based on physiognomic analysis (CLAMP) of leaf fossils from the Early Eocene Otaio Gorge section (this paper) and Early Palaeocene western South Island [*Kennedy*, 2003].

produced a MAT from the Otaio leaves of 21.6 ± 3.4°C (Table 1). The uncertainty reflects the sampling error [*Wilf*, 1997], and this is high because of the low diversity of the current Otaio collection. The LMA regression equation based on modern Australian data [*Greenwood et al.*, 2004] produced a MAT estimate for Otaio of 16.0 ± 3.0°C, with a range of 13.0–19.0°C. CLAMP analyses yielded an MAT estimate of 20.0 ± 2.4°C. Other CLAMP estimates indicate moderate seasonality, with mild winter temps (Coldest Mean Monthly Temperature range: 7.3–14.8°C, 2 stand-ard deviations), warm summer temps (Warmest Mean Monthly Temperature range: 25.5–31.8°C, 2 standard deviations), and a long growing season (supporting information Table S1). These values are similar to the preliminary results that were published in *Huber and Caballero* [2011]. Interestingly, the LMA-derived MAT estimate (Australian calibration) compares well with the estimate derived from bioclimatic analysis, whereas the warmer CLAMP-derived and LMA-derived (SE Asian calibration) MATs agree with the MBT'-CBT estimate (Figure 8b).

[33] Good agreement between MAT estimates derived from palynological and paleobotanical methods and MBT′-CBT-derived MATs from the New Zealand sections, ODP Site 1172 and IODP Site U1356 gives us considerable confidence in these results.

3.2.2. Comparison of MAT and SST Records

[34] These MAT estimate are markedly lower than SSTs derived from TEX_{86}^H values [*Bijl et al.*, 2009; *Hollis et al.*, 2009, 2012]. Caution is required when comparing MAT to SST, as differences can arise from a range of factors. For example, low MAT could reflect a high-altitude source region for the branched GDGTs [*Bendle et al.*, 2010], whereas high SST could be due to a summer bias in the marine proxies [e.g., *Sluijs et al.*, 2006; *Huber and Caballero*, 2011; *Hollis et al.*, 2012] as has been invoked for several Plio-Pleistocene studies [e.g., *Castaneda et al.*, 2010; *Huguet et al.*, 2006; *Menzel et al.*, 2006]. TEX_{86}^H-based SSTs are higher than SSTs based on the TEX_{86}^L calibration as well as those based on inorganic SST proxies [*Hollis et al.*, 2012]. This led to a proposed "paleocalibration" for TEX_{86} ($pTEX_{86}$) [*Hollis et al.*, 2012], which yields temperatures similar TEX_{86}^L-derived SSTs in SW Pacific sites and closer to the MATs derived for the Canterbury Basin sections (Figure 8a). These offsets between the TEX_{86}^L and TEX_{86}^H calibrations could arise from issues associated with the depth of GDGT production and export [*Taylor et al.*, 2013], and TEX_{86}^L and $pTEX_{86}$ appear to better represent marine temperatures in these settings [*Hollis et al.*, 2012].

[35] As discussed above, TEX_{86}^L-derived SSTs and MBT′-CBT-derived MATs are similar in the Paleocene and upper Middle Eocene sections, differing by less than 3°C, which is well within the combined calibration errors (Figures 7a and 7b). However, Early to early Middle Eocene (56–47 Ma) SSTs are consistently higher than corresponding MATs in the Mid-Waipara section and at ODP Site 1172. One of the challenges in making such comparisons is the large calibration errors of ±2.5–5°C that are associated with GDGT-based temperature proxies. We can partially circumvent this by comparing variations in relative temperature from the mean value (Figure 7b). This reveals that TEX_{86}^L-SST (but also TEX_{86}^H-and $pTEX_{86}$, not shown) and MBT′-CBT-MAT exhibit markedly similar temporal trends, giving us some confidence in them as relative temperature indicators. Both proxies show pronounced warming through

the Paleocene-Eocene transition, with Eocene temperatures being ~8–10°C warmer than the Paleocene. Both proxies also record a significant cooling event in the early Late Paleocene, with temperatures ~3°C lower than background Paleocene.

[36] The proxies diverge in the EECO, however, with SST ~5°C warmer than MAT. In fact, in the MAT records for the mid-Waipara section and ODP Site 1172, the EECO does not stand out as markedly warmer than much of the Middle Eocene (Figure 8). This could be due to a range of proxy-specific factors. For example, during the EECO, the source region from which branched GDGTs and pollen derive could have changed from lowlands to uplands, mitigating the MAT trends; however, it seems unlikely that such catchment-specific mechanisms would have impacted both sites. It is also possible that sedimentary marine production of branched GDGTs has biased MAT estimates during the EECO, which would be consistent with the relatively low BIT indices in that interval (Figure 7c). However, this also seems untenable because the EECO BIT indices are similar to those in Paleocene sediments. We also note that for CBT values of 0.8 (as observed during the EECO), the maximum MAT that can be obtained using the MBT′-CBT proxy (i.e., for an MBT value of 1) is 27°C [*Peterse et al.*, 2012]. This potential limitation requires future consideration, especially if the proxy is applied to lower latitude settings during greenhouse climate intervals.

[37] However, the MBT′-CBT-derived MATs for the EECO agree with (within error) or are even slightly higher than the MATs obtained from bioclimatic analysis of sporomorph assemblages (Figure 8). We do not have pollen data from Waipara for the later Middle Eocene, but pollen data from Middle Eocene strata elsewhere in New Zealand suggest a cooling in the late Middle Eocene, seen especially in increased abundance of *Nothofagus* pollen [*Raine et al.*, 2009]. However, the continued presence of *Nypa* pollen until the Late Eocene suggests that temperature did not drop to Paleocene levels.

[38] In summary, we observe good correspondence between MAT records in the SW Pacific and Wilkes Land margin but there may be a partial decoupling of air and sea surface temperatures for the SW Pacific [*Bijl et al.*, 2013]. By extension, the particularly pronounced high-latitude SST warming in this region (Figures 7 and 8) [*Hollis et al.*, 2012; *Bijl et al.*, 2013] during the EECO (and

specifically from 54 to 47 Ma) represents a stronger oceanic response to warming than an atmospheric one. This could have been due to a particularly strong influence of regional ocean currents on SSTs [*Hollis et al.*, 2012] as discussed below.

4. Integration of Temperature Records

[39] MAT estimates range from 13 to 15°C (with a calibration error of ±5°C) in the Paleocene from 62 to ~59 Ma. In the early Late Paleocene sediments, MAT decreases to a minimum of 10°C. This Late Paleocene cool interval indicates that the cooling inferred from TEX_{86} in the same section [*Hollis et al.*, 2012] was not limited to the marine realm. Crucially, these low Paleocene temperatures place an upper limit on mid-Paleocene Antarctic temperature and have implications for ice and permafrost accumulation. MATs in New Zealand of 10–15 ± 5°C are consistent with climate simulations that allow accumulation of permafrost on Antarctica (using 900 ppm pCO_2 and an equilibrium orbital configuration, which yields NZ surface temperatures of 10–15°C) [*DeConto et al.*, 2012; R. DeConto, personal communication, 2013]. Such deposits have been invoked as a potential source of light carbon released during the PETM [*DeConto et al.*, 2012]. We note, however, that we lack data from between 58 and 56 Ma, and warming during that time, which is evident in the benthic foraminiferal oxygen isotope record [e.g., *Cramer et al.*, 2011], could have led to permafrost thaw before the PETM. Nonetheless, the reconstructed MATs, taking into account their ±5°C error, are consistent with a cold Antarctic continent during much of the Paleocene.

[40] Following the Late Paleocene cool interval, MAT estimates increase dramatically at the PETM to 23°C. MAT estimates are also relatively high, ~19–22°C, from 51 to 46 Ma. Similar elevated MAT estimates occur at ODP Site 1172, indicating that both the PETM and EECO were characterized by cool subtropical temperatures in these high-latitude terrestrial settings as first recognized some forty years ago by *Shackleton and Kennett* [1975]. The EECO MATs for mid-Waipara and ODP Site 1172 are similar to those obtained for Wilkes Land, East Antarctica, also determined using a combination of palynological and recalculated MBT′-CBT proxies [*Pross et al.*, 2012, Figure 8b]. Low tropic to pole SST gradients have been suggested for the EECO [*Greenwood and Wing*, 1995; *Pearson et al.*, 2007; *Bijl et al.*, 2009; *Hollis et al.*, 2009, 2012], but these MBT′-CBT

records indicate that temperature gradients were minimal even at high latitudes, between New Zealand and Antarctica, at least until the Middle Eocene [see also *Bijl et al.*, 2013].

[41] The New Zealand, ODP Site 1172 and Antarctic EECO MAT and $TEX_{86}{}^{L}$-derived SSTs are all markedly lower than the original TEX_{86}-SSTs. Therefore, they yield higher latitudinal temperature gradients and partially resolve data-climate model discrepancies [*Huber and Caballero*, 2011]. For example, a simulation with 16 × CO_2 [*Huber and Caballero*, 2011] yields tropical SST near Tanzania of 35–40°C and SW Pacific MAT of 15–25°C. These modeled tropical temperatures are within the error range of recalculated Tanzanian SSTs ($TEX_{86}{}^{H}$ = 33–35 ± 2.5°C; planktic foraminiferal $\delta^{18}O$ = 32–33 ± 2°C; SI of *Hollis et al.* [2012]). The modeled Australia/NZ MAT range is admittedly large, but it does bracket our reconstructed MATs (19–22 ± 5°C) and SSTs (25–27.5 ± 4°C). Therefore, our data provide evidence for a reduced latitudinal temperature gradient during the EECO that is consistent with physical climate models. This implies that the current generation of models are approaching, although not altogether achieving, the appropriate level of polar amplification needed to match proxy data, under conditions of extremely high pCO_2 or high climate sensitivity [*Lunt et al.*, 2012; *Huber and Caballero*, 2011].

[42] From late Early to early Middle Eocene, New Zealand MATs are relatively stable, and it is only at ~42 Ma that lower MATs of 17–19°C are observed (Figure 8b; difference between MATs from 42–41 to 52–45 Ma confirmed by *t* Test). Similar MAT trends are evident at ODP Site 1172 (Figure 8b), although that section exhibits a more gradual cooling from 46 to 42 Ma (different EECO and Middle Eocene MATs confirmed by *t* Test). Both MAT records contrast with that from Wilkes Land, which exhibits ~5°C lower MATs already by 48 Ma [*Pross et al.*, 2012]. As discussed above, the stable New Zealand and Site 1172 MATs from ~52 to 45 Ma contrast with the corresponding SST records (Figure 7) and could be the result of branched GDGT (and sporomorph) transport dynamics. If they are unbiased, however, the MAT records document the development of a strong temperature gradient between New Zealand/ODP Site 1172 and the Antarctic coast at the Early-Middle Eocene boundary [this work; *Bijl et al.*, 2013]. This suggests the initiation of a proto-Antarctic frontal system, which could have been caused by global climate drivers such as a decrease in pCO_2. Alternatively, it could have been brought

about by tectonic mechanisms, such as an early phase in the opening of the Tasman Gateway, as has been argued by *Bijl et al.* [2011, 2013].

[43] These or related oceanographic processes could also explain the apparent decoupling between SST and MAT reconstructions for both New Zealand and ODP Site 1172. The present-day East Australian Current (EAC) is a western boundary current that delivers warm subtropical water circulation to the Tasman Sea and SW Pacific (~45°S) [*Ridgway and Hill*, 2009]. Near-future modeling experiments indicate that global warming can cause this current to extend as far south as 54°S, the extent being controlled by the westerly wind belt, geography and conservation of angular momentum [*Cai et al.*, 2005; *Wu et al.*, 2012]. Therefore, it is conceivable that during episodes of extreme greenhouse warming, the EAC could warm surface waters at the edges of the Australia and New Zealand landmasses and cause MAT-SST decoupling. If so, the reduced offset between SST and MAT after 47 Ma (Figure 7b) would be consistent with evidence of little EAC influence in the Middle Eocene at ODP Site 1172 [*Bijl et al.*, 2013]. However, southward expansion of the EAC to the Australian and New Zealand landmasses (at ~65 and ~55°S, respectively) does not occur in EECO climate simulations [*Huber and Nof*, 2006; *Ali and Huber*, 2010], and additional coupled MAT and SST data sets are required to examine SW Pacific palaeoceanography further.

[44] In summary, our MBT'-CBT and floral-derived MAT estimates from New Zealand show that: (i) the EECO and PETM were significantly warmer than the Paleocene; (ii) subtropical conditions prevailed in southern New Zealand during the EECO and early Middle Eocene; and (iii) there was a minimal temperature gradient between New Zealand and the Antarctic region during the EECO but that a significant gradient in MAT developed at about 48 Ma. These results are consistent with climate models that show an increase in temperature gradient with decreasing global mean surface temperature [*Huber and Caballero*, 2011; *Lunt et al.*, 2012].

5. Conclusions

[45] Our long-term record of Early Paleogene MAT provides an important addition to previous investigations of middle and high-latitude South Pacific climate. There is good agreement between relative temperature trends in MAT and SST, with absolute mean air temperature estimates being

consistent with recently revised SSTs records [*Hollis et al.*, 2012]. While this new SW Pacific temperature record for the Early Paleogene still suggests pronounced warming and reduced latitudinal gradients during times of peak global warmth, such as the PETM and EECO, it does not support the extreme temperatures in previous publications. Crucially, climate simulations with high pCO_2 levels [e.g., *Huber and Caballero*, 2011; *Lunt et al.*, 2012] can reproduce these MATs on the New Zealand and Australian landmasses as well as approximating previously reported tropical SSTs (within 2–5°C). Arguably of even greater significance than the warm Eocene is the remarkable evidence for cooling in early Late Paleocene, which suggests that an as yet unidentified climate driver caused Southwest Pacific temperatures to plummet to levels barely warmer than the present day.

Acknowledgments

References

Ali, J. R., and M. Huber (2010), Mammalian biodiversity on Madagascar controlled by ocean currents, *Nature*, *463*, 653–656.

Australian National Herbarium Specimen Information Register (2011), Centre for Australian National Biodiversity Research. [Available at http://www.anbg.gov.au/cpbr/program/hc/hc-ANHSIR.html].

Beerling, D. J., and D. L. Royer (2011), Convergent Cenozoic CO_2 history. *Nature Geosci.*, *4*, 418–420.

Bendle, J. A., J. W. H. Weijers, M. A. Maslin, J. S. Sinninghe Damsté, S. Schouten, E. C. Hopmans, C. S. Boot, and R. D. Pancost (2010), Major changes in glacial and Holocene terrestrial temperatures and sources of organic carbon recorded in the Amazon fan by tetraether lipids, *Geochem. Geophys. Geosyst.*, *11*, Q12007, doi:10.1029/2010GC003308.

Bijl, P. K., S. Schouten, A. Sluijs, G.-J. Reichart, J. C. Zachos, and H. Brinkhuis (2009), Early Palaeogene temperature evolution of the southwest Pacific Ocean, *Nature*, *461*, 776–779.

Bijl, P. K., J. Pross, J. Warnaar, C. E. Stickley, M. Huber, R. Guerstein, A. J. P. Houben, A. Sluijs, H. Visscher, and H. Brinkhuis (2011), Environmental forcings of Paleogene

Southern Ocean dinoflagellate biogeography, *Paleoceanography*, *26*, PA1202, doi:10.1029/2009PA001905.

Bijl, P. K., et al. (2013), Eocene cooling linked to early flow across the Tasmnian Gateway, *Proc. Natl. Acad. Sci. U. S. A.*, *110*(24), 9645–9650, doi:10.1073/pnas.1220872110.

Burgess, C. E., P. N. Pearson, C. H. Lear, H. E. G. Morgans, L. Handley, R. D. Pancost, and S. Schouten (2008), Middle Eocene climate cyclicity in the southern Pacific: Implications for global ice volume, *Geology*, *36*, 651–654.

Cai, W., G. Shi, T. Cowan, D. Bi, and J. Ribbe (2005), The response of the Southern Annular Mode, the East Australian Current, and the southern mid-latitude ocean circulation to global warming, *Geophys. Res. Lett.*, *32*, L23706, doi:10.1029/2005GL024701.

Castaneda, I. S., E. Schefuss, J. Patzold, J. S. Sinninghe Damsté, S. Weldeab, and S. Schouten (2010), Millennial-scale sea surface temperature changes in the eastern Mediterranean (Nile River Delta region) over the last 27,000 years, *Paleoceanography*, *25*, PA1208, doi:10.1029/2009pa001740.

Contreras, L., J. Pross, P. K. Bijl, A. Koutsodendris, J. I. Raine, B. van de Schootbrugge, and H. Brinkhuis (2013), Early to middle Eocene vegetation dynamics at the Wilkes Land Margin (East Antarctica), *Rev. Palaeobot. Palynol.*, *197*, 119–142.

Cramer, B. S., K. G. Miller, P. J. Barrett, and J. D. Wright (2011), Late Cretaceous-Neogene trends in deep ocean temperature and continental ice volume: Reconciling records of benthic foraminiferal geochemistry ($\delta^{18}O$ and Mg/Ca) with sea level history, *J. Geophys. Res.*, *116*, C12023, doi:10.1029/2011JC007255.

Creech, J. B., J. A. Baker, C. J. Hollis, H. E. G. Morgans, and E. G. C. Smith (2010), Eocene sea temperatures for the mid-latitude southwest Pacific from Mg/Ca ratios in planktonic and benthic foraminifera, *Earth Planet. Sci. Lett.*, *299*, 483–495.

Crouch, E. M., and H. Brinkhuis (2005), Environmental change across the Paleocene-Eocene transition from eastern New Zealand: A marine palynological approach, *Mar. Micropaleontol.*, *56*, 138–160.

DeConto, R. M., S. Galeotti, M. Pagani, D. Tracy, K. Schaefer, T. Zhang, D. Pollard, and D. J. Beerling (2012), Past extreme warming events linked to massive carbon release from thawing permafrost, *Nature*, *484*, 87–90.

Eglinton, G., R. A. Raphael, A. G. Gonzalez, and R. J. Hamilton (1962), Hydrocarbon constituents of wax coatings of plant leaves—A taxonomic survey, *Nature*, *193*, 739–742.

Fietz, S., F. G. Prahl, N. Moraleda, and A. Rosell-Melé (2013), Eolian transport of glycerol dialkyl glycerol tetraethers (GDGTs) off northwest Africa, *Org. Geochem.*, *64*, 112–118.

Forsythe, P. J. (2001), *Institute of Geological and Nuclear Sciences Geological Map, sheet 19, scale 1:250,000*, Inst. of Geol. and Nucl. Sci. Ltd., Lower Hutt, New Zealand.

Gradstein F. M., J. G. Ogg, and F. J. Hilgen (2012), On the Geologic Time Scale. *Newsletters on Stratigraphy*, *45*, 171–188.

Greenwood, D. R., and S. L. Wing (1995), Eocene continental climates and latitudinal temperature-gradients, *Geology*, *23*, 1044–1048.

Greenwood, D. R., P. Wilf, S. L. Wing, and D. C. Christophel (2004), Paleotemperature estimates using Leaf-Margin Analysis: Is Australia different?, *Palaios*, *19*, 129–142.

Greenwood, D. R., S. B. Archibald, R. W. Mathewes, and P. T. Moss (2005), Fossil biotas from the Okanagan Highlands, southern British Columbia and northeastern Washington State: Climates and ecosystems across an Eocene landscape, *Can. J. Earth Sci.*, *42*, 167–185.

Hollis, C. J., et al. (2009), Tropical sea temperatures in the high-latitude South Pacific during the Eocene, *Geology*, *37*, 99–102.

Hollis, C. J., et al. (2012), Early Paleogene temperature history of the Southwest Pacific Ocean: Reconciling proxies and models, *Earth Planet. Sci. Lett.*, *349*, 53–66.

Hopmans, E. C., J. W. H. Weijers, E. Schefuss, L. Herfort, S. D. Sinninghe Damsté, and S. Schouten (2004), A novel proxy for terrestrial organic matter in sediments based on branched and isoprenoid tetraether lipids, *Earth Planet. Sci. Lett.*, *224*, 107–116.

Houlder, D., M. Hutchinson, H. Nix, and J. McMahon (1999), *ANUCLIM User's Guide*, Centre for Resource and Environmental Studies (CRES). Australian National Univ., Canberra, Australia.

Huber, M., and R. Caballero (2011), The early Eocene equable climate problem revisited, *Clim. Past*, *7*, 603–633.

Huber, M., and D. Nof (2006), The ocean circulation in the southern hemisphere and its climatic impacts in the Eocene, *Palaeogeogr. Palaeoclimatol. Palaeoecol.*, *231*, 9–28.

Huguet, C., J. H. Kim, J. S. Sinninghe Damsté, and S. Schouten (2006), Reconstruction of sea surface temperature variations in the Arabian Sea over the last 23 kyr using organic proxies (TEX_{86} and $U^{K'}_{37}$), *Paleoceanography*, *21*, PA3003, doi:10.1029/2005pa001215.

Kennedy, E. M. (2003), Late Cretaceous and Paleocene terrestrial climates of New Zealand: Leaf fossil evidence from South Island assemblages, *N. Z. J. Geol. Geophys.*, *46*, 295–306.

Kim, J. H., J. van der Meer, S. Schouten, P. Helmke, V. Willmott, F. Sangiorgi, N. Koc, E. C. Hopmans, and J. S. Sinninghe Damsté (2010), New indices and calibrations derived from the distribution of crenarchaeal isoprenoid tetraether lipids: Implications for past sea surface temperature reconstructions, *Geochim. Cosmochim. Acta*, *74*, 4639–4654.

Kolattukudy, P. E. (1976), *The Chemistry and Biochemistry of Natural Waxes*, Elsevier, Amsterdam.

Lear, C. H., H. Elderfield, and P. A. Wilson (2000), Cenozoic deep-sea temperatures and global ice volumes from Mg/Ca in benthic foraminiferal calcite, *Science*, *287*, 269–272.

Liu Z., M. Pagani, D. Zinniker, R. DeConto, M. Huber, H. Brinkhuis, S. R. Shah, R. M. Leckie, and A. Pearson (2009), Global cooling during the Eocene-Oligocene climate transition. *Science*, *323*, 1187–1190.

Lunt, D. J., et al. (2012), A model-data comparison for a multi-model ensemble of early Eocene atmosphere-ocean simulations: EoMIP, *Clim. Past*, *8*, 1717–1736.

Menzel, D., E. C. Hopmans, S. Schouten, and J. S. Sinninghe Damsté (2006), Membrane tetraether lipids of planktonic Crenarchaeota in Pliocene sapropels of the eastern Mediterranean Sea, *Palaeogeogr. Palaeoclimatol. Palaeoecol.*, *239*, 1–15.

Mildenhall, D. C. (1980), New Zealand Late Cretaceous and Cenozoic plant biogeography—A contribution, *Palaeogeogr. Palaeoclimatol. Palaeoecol.*, *31*, 197–233.

Morgans, H. E. G. (2009), Late Paleocene to middle Eocene foraminiferal biostratigraphy of the Hampden Beach section, eastern South Island, New Zealand, *N. Z. J. Geol. Geophys.*, *52*, 273–320.

Morgans, H. E. G., C. M. Jones, E. M. Crouch, B. D. Field, C. J. Hollis, J. I. Raine, C. P. Strong, and G. J. Wilson (2004), Upper Cretaceous to Eocene stratigraphy and sample collections, mid-Waipara River section, North Canterbury, *Sci. Rep. 2003/08*, Inst. Geol. and Nucl. Sci., Wellington NZ, 101 pp.

Mosbrugger, V., and T. Utescher (1997), The coexistence approach—A method for quantitative reconstructions of Tertiary terrestrial palaeoclimate data using plant fossils, *Palaeogeogr. Palaeoclimatol. Palaeoecol.*, *134*, 61–86.

Pagani, M., J. C. Zachos, K. H. Freeman, B. Tipple, and S. Bohaty (2005), Marked decline in atmospheric carbon dioxide concentrations during the Paleogene, *Science*, *309*, 600–603.

Pagani, M., M. Huber, Z. H. Liu, S. M. Bohaty, J. Henderiks, W. Sijp, S. Krishnan, and R. M. DeConto (2011), The role of carbon dioxide during the onset of Antarctic glaciation, *Science*, *334*, 1261–1264.

Pearson, P. N., and M. R. Palmer (2000), Atmospheric carbon dioxide concentrations over the past 60 million years, *Nature*, *406*, 695–699.

Pearson, P. N., B. E. van Dongen, C. J. Nicholas, R. D. Pancost, S. Schouten, J. M. Singano, and B. S. Wade (2007), Stable warm tropical climate through the Eocene Epoch, *Geology*, *35*, 211–214.

Peterse, F., J. H. Kim, S. Schouten, D. K. Kristensen, N. Koc, and J. S. Sinninghe Damsté (2009), Constraints on the application of the MBT/CBT palaeothermometer at high latitude environments (Svalbard, Norway), *Org. Geochem.*, *40*, 692–699.

Peterse, F., J. van der Meer, S. Schouten, J. W. H. Weijers, N. Fierer, R. B. Jackson, J.-H. Kim, and J. S. Sinninghe Damsté (2012), Revised calibration of the MBT-CBT paleotemperature proxy based on branched tetraether membrane lipids in surface soils, *Geochim. Cosmochim. Acta*, *96*, 215–229.

Pocknall, D. T. (1990), Palynological evidence for the early to middle Eocene vegetation and climate history of New Zealand, *Rev. Palaeobot. Palynol.*, *65*, 57–69.

Pole, M. (1994), An Eocene macroflora from the Taratu Formation at Livingston, North Otago, New Zealand, *Aust. J. Bot.*, *42*, 341–367.

Pole, M. (1997), Paleocene plant macrofossils from Kakahu, South Canterbury, New Zealand, *J. R. Soc. N. Z.*, *27*, 371–400.

Pole, M. (2010), Ecology of Paleocene-Eocene vegetation at Kakahu, South Canterbury, New Zealand, *Palaeontol. Electron.*, *13*(2), 29.

Pross, J., S. Klotz, and V. Mosbrugger (2000), Reconstructing palaeotemperatures for the Early and Middle Pleistocene using the mutual climatic range method based on plant fossils, *Quat. Sci. Rev.*, *19*, 1785–1799.

Pross, J., et al. (2012), Persistent near-tropical warmth on the Antarctic continent during the early Eocene epoch, *Nature*, *488*, 73–77.

Raine, J. I., E. M. Kennedy, and E. M. Crouch (2009), New Zealand Paleogene vegetation and climate, in *Climatic and Biotic Events of the Paleogene (CBEP 2009), Extended Abstracts From an International Conference in Wellington, New Zealand*, *GNS Sci. Misc. Ser.*, vol. *18*, edited by E. M. Crouch, C. P. Strong, and C. J. Hollis, Wellington NZ, pp. 117–122.

Reiley, G., R. J. Collier, D. M. Jones, and G. Eglinton (1991), The biogeochemistry of Ellesmere Lake, UK. I: Source correlation of leaf wax inputs to the sedimentary record, *Org. Geochem.*, *17*, 902–912.

Ridgway, K., and K. Hill (2009), The East Australian Current, in *A Marine Climate Change Impacts and Adaptation Report Card for Australia 2009*, edited by E. S. Poloczanska, A. J. Hobday, and A. J. Richardson, NCCARF Publication 05/09, Natl. Clim. Change Adoptation Res. Facil, NCAARF.

Scalan, R. S., and J. E. Smith (1970), An improved measure of the odd-to-even predominance in the normal alkanes of sediment extracts and petroleum, *Geochim. Cosmochim. Acta*, *34*, 611–620.

Schouten, S., E. C. Hopmans, E. Schefuss, and J. S. Sinninghe Damsté (2002), Distributional variations in marine crenarchaeotal membrane lipids: A new tool for reconstructing ancient sea water temperatures?, *Earth Planet. Sci. Lett.*, *204*, 265–274.

Sinninghe Damsté, J. S., J. Ossebaar, S. Schouten, and D. Verschuren (2008), Altitudinal shifts in the branched tetraether lipid distribution in soil from Mt. Kilimanjaro (Tanzania): Implications for the MBT/CBT continental palaeothermometer, *Org. Geochem.*, *39*, 1072–1076.

Sluijs, A., et al. (2006), Subtropical arctic ocean temperatures during the Palaeocene/Eocene thermal maximum, *Nature*, *441*, 610–613.

Spicer, R. A., P. J. Valdes, T. E. V. Spicer, H. J. Craggs, G. Srivastava, R. C. Mehrotra, and J. Yang (2009), New developments in CLAMP: Calibration using global gridded meteorological data. *Palaeogeogr. Palaeoclimatol. Palaeoecol.*, *283*, 91–98.

Taylor, K. W. R., M. Huber, C. J. Hollis, M.-T. Hernandez-Sanchez, and R. D. Pancost (2013), Re-evaluating modern and Palaeogene GDGT distributions: Implications for SST reconstructions, *Global Planet. Change*, *108*, 158–174.

ter Braak, C. J. F. (1986), Canonical correspondence analysis: A new eigenvector technique for multivariate direct gradient analysis, *Ecology*, *67*, 1167–1179.

Utescher, T., and V. Mosbrugger (2013), The Palaeoflora Database. Universität Bonn, Bonn. [Available at http://www.geologie.unibonn.de/Palaeoflora.]

Weijers, J. W. H., S. Schouten, J. C. van den Donker, E. C. Hopmans, and J. S. Sinninghe Damsté (2007a), Environmental controls on bacterial tetraether membrane lipid distribution in soils, *Geochim. Cosmochim. Acta*, *71*, 703–713.

Wilf, P. (1997), When are leaves good thermometers? A new case for Leaf Margin Analysis, *Paleobiology*, *23*, 373–390.

Wing, S. L., and D. R. Greenwood (1993), Fossils and fossil climate: The case for equable continental interiors in the Eocene, *Philos. Trans. R. Soc. B*, *341*, 243–252.

Wolfe, J. A. (1979), Temperature parameters of humid to Mesic forests of Eastern Asia and relation to forests of other regions of the Northern Hemisphere and Australasia, *U.S. Geol. Surv. Prof. Pap.*, *1106*, 1–37.

Wolfe, J. A. (1993) A method of obtaining climatic parameters from leaf assemblages, *U.S. Geol. Surv. Bull.*, *2040*, 71.

Wu, L., W. Cai, L. Zhang, H. Nakamura, A. Timmermann, T. Joyce, M. J. McPhaden, M. Alexander, B. Qiu, M. Visbeck, P. Chang, and B. Giese (2012), Enhanced warming over the global subtropical western boundary currents, *Nat. Clim. Change*, *2*, 161–166.

Yang, H., R.D. Pancost, X. Dang, X. Zhou, R.P. Evershed, G. Xiao, C. Tang, L. Gao, Z. Guo, and S. Xie (2013), Correlations between microbial tetraether lipids and environmental variables in Chinese soils: Optimizing the paleo-reconstructions in semi-arid and arid regions. *Geochimica Cosmochimica Acta.*, *126*, 49–69.

Zachos, J., M. Pagani, L. Sloan, E. Thomas, and K. Billups (2001), Trends, rhythms, and aberrations in global climate 65 Ma to present, *Science*, *292*, 686–693.

Zachos, J. C., G. R. Dickens, and R. E. Zeebe (2008), An early Cenozoic perspective on greenhouse warming and carbon-cycle dynamics, *Nature*, *451*, 279–283.

Zhu, C., J. W. H. Weijers, T. Wagner, J. M. Pan, J. F. Chen, and R. D. Pancost (2011), Sources and distributions of tetraether lipids in surface sediments across a large river-dominated continental margin, *Org. Geochem.*, *42*, 376–386.